

Manipulation of electronic and magnetic properties of M_2C (M=Hf, Nb, Sc, Ta, Ti, V, Zr) monolayer by applying mechanical strains

Shijun Zhao,^{1,2} Wei Kang,^{1,2,*} and Jianming Xue^{1,3}

¹*HEDPS, Center for Applied Physics and Technology,
Peking University, Beijing 100871, P. R. China*

²*College of Engineering, Peking University, Beijing 100871, P. R. China*

³*State Key Laboratory of Nuclear Physics and Technology,
School of Physics, Peking University, Beijing 100871, P. R. China*

Tuning the electronic and magnetic properties of a material through strain engineering is an effective strategy to enhance the performance of electronic and spintronic devices. Recently synthesized two-dimensional transition metal carbides M_2C (M=Hf, Nb, Sc, Ta, Ti, V, Zr), known as MXenes, has aroused increasingly attentions in nanoelectronic technology due to their unusual properties. In this paper, first-principles calculations based on density functional theory are carried out to investigate the electronic and magnetic properties of M_2C subjected to biaxial symmetric mechanical strains. At the strain-free state, all these MXenes exhibit no spontaneous magnetism except for Ti_2C and Zr_2C which show a magnetic moment of 1.92 and 1.25 μ_B /unit, respectively. As the tensile strain increases, the magnetic moments of MXenes are greatly enhanced and a transition from nonmagnetism to ferromagnetism is observed for those nonmagnetic MXenes at zero strains. The most distinct transition is found in Hf_2C , in which the magnetic moment is elevated to 1.5 μ_B /unit at a strain of 1.80%. We further show that the magnetic properties of Hf_2C are attributed to the band shift mainly composed of Hf(5d) states. This strain-tunable magnetism can be utilized to design future spintronics based on MXenes.

Two-dimensional (2D) materials have attracted a great deal of attention due to their unique mechanical and electronic properties and numerous potential applications.¹ Very recently, a family of 2D materials was synthesized by the exfoliation of the layered ternary transition metal carbides, which are known as MAX phase.^{2,3} The MAX phases represent a large (more than 60 members) family of ternary layered machinable transition metal carbides, nitrides, and carbonitrides, which possess unique properties such as remarkable machinability, high damage tolerance, excellent oxidation resistance, and high electrical as well as thermal conductivity.^{4,5} The MAX phases are layered hexagonal (space group $P63/mmc$) with the formula of $M_{n+1}AX_n$ ($n=1,2,3$), where M represents an early transition metal, A is an A-group element (mostly groups IIIA and IVA) and X denotes carbon or nitrogen. The layered structure makes the exfoliation of MAX phase feasible and by removal of the A group layer from the MAX phase, 2D MXenes can be obtained which share the structural similarities with graphene.^{6,7}

The extraordinary properties of 2D MXenes have been intensely investigated since its successful synthesis experimentally.⁶⁻¹⁴ High conductivities and high elastic moduli are found in MXenes.⁶⁻⁸ Besides, the applications of MXenes in Li-ion battery anodes and hybrid electrochemical capacitors are also demonstrated.^{9,10} Most of the synthesized $M_{n+1}X_n$ layers are metallic with no band gap, although it is shown that the electronic structure can be modulated by appropriate surface terminations such as oxygen and fluoride.^{6,15} However, previous theoretical studies indicate that the majority of the functionalized MXene systems are nonmagnetic. For the “pure” MXenes, only the $Ti_{n+1}X_n$ (X=C,N) monolayers are magnetic due to the 3d electrons of surface Ti atoms.¹⁶

In the applications based on nanoelectronic devices, an essential requirement is the versatile ability to modulate the electronic and magnetic properties via external controls. It has been well established that the electronic and magnetic properties of materials can be tuned by applying mechanical strains.^{17,18} In particular, the effects of strain will be more significant in 2D systems as demonstrated in graphene and other transition metal chalcogenides such as MoS_2 , NbS_2 , $NbSe_2$ and VSe_2 .^{17,19} For example, a uniaxial strain larger than 20% applied in graphene along the zigzag direction is predicted to open a bandgap due to level crossing.²⁰ Different from bulk materials in which strains can be relaxed by dislocation plasticity or fracture, 2D materials are well suited for strain engineering. From experimental view point, strain in 2D sheet can be achieved rather easily by manipulating its substrate.

In the present work, therefore, we study the effect of mechanical strains on the electronic properties of MXenes of the form M_2C (M=Hf, Nb, Sc, Ta, Ti, V, Zr). The influence of homogeneous biaxial tensile strain on these MXenes are systematically investigated based on density functional theory calculations. Our results demonstrate that the Hf_2C structure can be efficiently magnetized by simply applying a tensile strain, during which the structures of MXenes are still maintained. The effect of compressive strain is not considered in the present work because it is impractical for experimental implementation.

Electronic structure calculations have been carried out using the density functional theory as implemented in the Vienna *ab initio* simulation (VASP) code.²¹ The electron-ion interactions are described by Projector-augmented-wave (PAW) pseudopotentials with semi-core states treated as valence states.²² The exchange

and correlation energies are treated within the generalized gradient approximation (GGA) according to PW91 parametrization.²³ To obtain the unstrained configuration of M_2X monolayer, both the atomic positions and lattice vectors are fully relaxed with the conjugate gradient algorithm to obtain the equilibrium lattice constant. The lattice constant is then increased gradually to model the biaxial strain, in which all atoms are optimized to calculate the electronic structure. The convergence for energy is chosen as 10^{-4} eV between two consecutive self-consistent steps and the atomic relaxation is performed until the interatomic forces are less than 0.01 eV/Å. A plane wave cutoff of 520 eV is used for all the calculations.

In our calculations, the M_2X is represented by a 4×4 supercell with a vacuum space of 18 Å between two adjacent layers to avoid interactions between periodic images of slabs in the z -direction. The Brillouin zone is sampled using a $6 \times 6 \times 1$ Monkhorst-Pack grid in relaxation calculations, while a denser mesh of $12 \times 12 \times 1$ is considered to generate density of states and charge densities.

The side and top views of generalized structure of M_2X MAXenes with hexagonal symmetry are illustrated in Fig. 1, which are constructed by removing ‘‘A’’ atoms from corresponding bulk MAX phases. In Fig. 1(b), the schematic illustration of the biaxial tensile strain are indicated. Here, the strain is defined as $\epsilon = (a - a_0)/a_0 = \Delta a/a_0$, where a_0 and a is the lattice parameter of the unstrained and strained supercell, respectively. As described previously, the structure of M_2X suggest that it can bear a relatively large range of in-plane elastic strains compared to the perfectly flat graphene and BN layer due to the possible deformation in the perpendicular direction.¹⁹

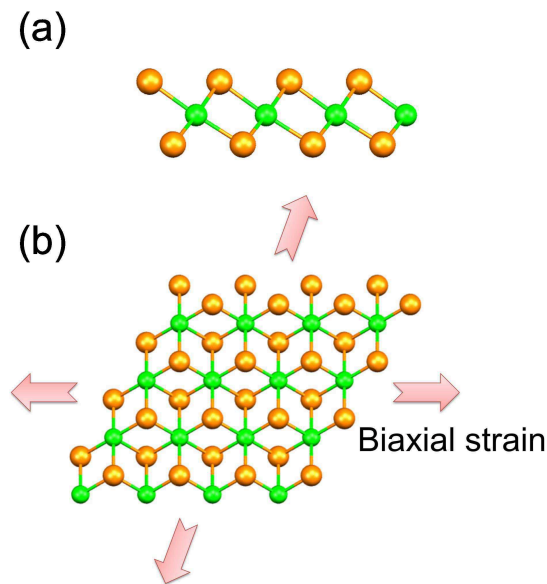


FIG. 1. (a) Side and (b) top view of M_2C , where the M and X atoms are denoted by orange and yellow spheres, respectively.

To study the effect of strain on the electronic properties of MXenes, we first relaxed the atomic positions as well as lattice vectors and obtained their optimized structures. The calculated lattice parameters of M_2X monolayer is summarized in Table I with available data from literatures shown for a comparison.

TABLE I. Lattice parameters (in Å) of M_2X monolayer determined with PW91 functional in this work. Available results from literatures computed from different functionals are also included for a comparison.

MXenes	Hf ₂ C	Nb ₂ C	Sc ₂ C	Ta ₂ C	Ti ₂ C	V ₂ C	Zr ₂ C
present	3.212	3.135	3.332	3.087	3.078	2.897	3.293
PBE ²⁴					3.076		
PBE ²⁵					3.0395		
DFTB ²⁶					3.33		
Wu-Cohen ²⁷	3.239			3.138	3.007	2.869	3.238

It can be seen that our results are in good agreement with available theoretical calculations, which also validates our approach in predicting the structural properties of these MXenes. Note that there is still no experimental values about the lattice parameters. Here it is helpful to make a comparison of these lattice constants with their corresponding MAX phases. Taking Ti_2AlC as an example, the lattice constant a of bulk Ti_2AlC is 3.065 Å determined from experiment,⁵ which is comparable to the calculated constant of Ti_2C as shown above. Therefore, it can be concluded that the structures of MXenes are almost the same as those in MAX phases.

After the stable structures of MXenes are obtained, we start to apply biaxial symmetric strains to the lattice to investigate the influence of strain on their electronic and magnetic properties. Previous theoretical calculations based on density functional theory have revealed that most of the MXenes are metallic. Indeed, our results demonstrate that all the investigated MXenes in this study are metallic system with no energy gap. This is still the case when strain is applied and the metallic properties of these MXenes are not changed. However, the magnetic properties are much affected. Here the total magnetic moment of MXenes as a function of applied strains are presented in Fig. 2.

As we can see, the magnetic properties of these MXenes can be effectively tuned by external strains. At the strain-free state, only the Ti_2C and Zr_2C has magnetic moment, which is 1.92 and $1.25 \mu_B$ /unit respectively. The results for Ti_2C is in good agreement with previous calculations of $1.85 \mu_B$ /unit.¹⁶ A noteworthy feature is that the Hf_2C display no magnetism although it is in the same group as Ti and Zr in the periodic table. In fact, it has been reported that in the MAX phase M_2AC , this group elements ($M=Ti, Zr$ and Hf) exhibit the lowest bulk moduli than other MAX phases. The reason is interpreted as the weak M d -orbital and C p -orbital bonding in these materials.²⁸ As the atomic number in-

creases, more carbon p electrons are participated in the M-C bonding. In the case of MXenes, the same trend is observed. The p orbital of carbon atom hybridizes weakly with d orbital of Ti, while a strong hybridization is observed between Hf($5d$) and C($2p$) orbitals. Therefore, the unsaturated Ti($3d$) dangling bonds lead to the magnetism in the Ti_2C monolayer. On the contrary, the strong bonding interaction between Hf and C gives rise to no magnetism in Hf_2C , which will be discussed in more details below.

All the magnetic moment of these MXenes are elevated by applied strains, although they show different behaviors. The most distinct variation is observed for Hf_2C , which turns from nonmagnetism to ferromagnetism with a high magnetic moment of $1.70 \mu_B/\text{unit}$ at a strain of 2%. In fact, the system becomes magnetic as long as the strain is applied, with a linearly increase of the magnetic moment. At about 6% strain, the spin moment increases slowly and remains almost constant for larger strains. This indicates that a slight variation of the strain applied on the Hf_2C layer can induce a large change of the spin moment.

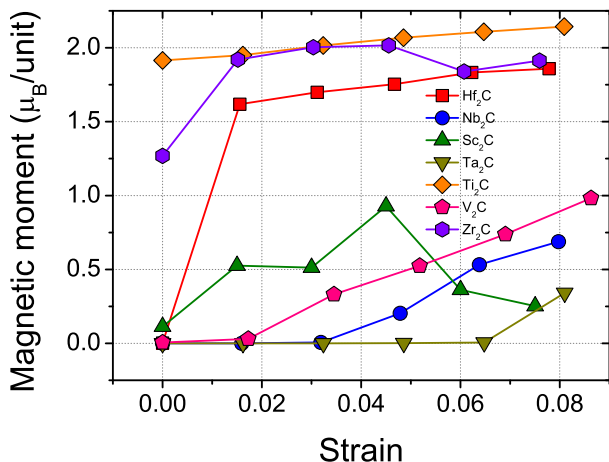


FIG. 2. Dependence of magnetic moments of various MXenes on the applied strain.

As a prototype of strain-engineered modulation on the magnetic properties of MXenes, we have made a detailed analysis on the interplay between the mechanical strain and the magnetic behaviors for Hf_2C . The magnetic moments of Hf and C atoms as a function of the applied strain is represented in Fig. 3(a). It is shown that the magnetic moment of Hf starts to increase sharply when the strain is applied and saturates to a value of $0.5 \mu_B/\text{atom}$ at a strain of 5%. The increase of magnetic moment in the strain range up to 2% is nearly linear with respect to the strain, which means that the magnetic property of Hf_2C is rather sensitive to the strain. On the other hand, the nonmagnetic property of C is not much influenced by the strain. These results suggest that the magnetism of Hf_2C under strains is mainly originated from Hf atoms.

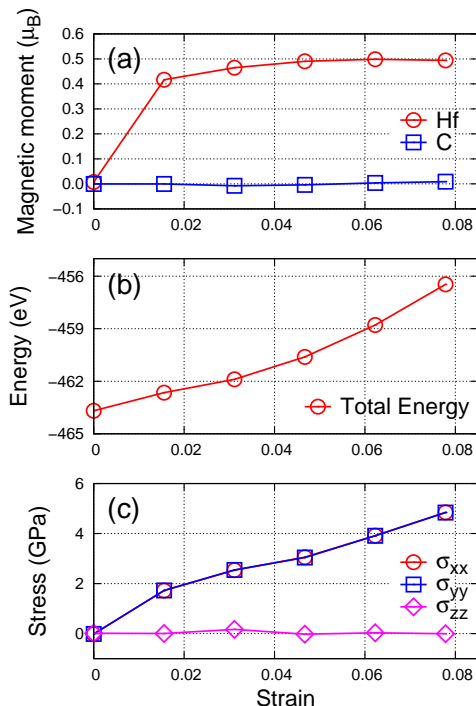


FIG. 3. Per atom magnetic moment, total energy and stress of Hf_2C as a function of applied strain.

In Fig. 3 (b) and (c), we have shown the dependence of the total energy and stress of Hf_2C sheet on the applied strain. The total energy is monotonically increased with strain, indicating the structure is still stable when it is subjected to these strains since no phase transition is observed. This implies that the Hf_2C monolayer can bear a large elastic strain range. The smoothly increase also suggests that the magnetic modulation is in the elastic range and reversible. This feature is significant for practical nanomechanical control of the properties of the MXenes system in device applications. The in-plane stresses of σ_{xx} and σ_{yy} are almost the same, which is the result of biaxial symmetric strains.

It is well established that the partially filled d character of the transition metal atoms can induce significant magnetism in materials. In our case, the magnetism is indeed induced by the Hf atom as demonstrated in Fig. 3. The Hf atom possesses two $5d$ electrons. However, due to the strong covalent interactions between Hf and C in the sandwiched structures, the monolayer MXene of Hf_2C exhibits no magnetism. This phenomena have been observed in other monolayer structures such as NbS_2 and NbSe_2 . In these materials, the strong ligand field owing to the covalent bonds tend to quench the magnetism of the transition metal. When external strain is applied, the covalent bonding interactions inside Hf_2C is reduced and result in the release of the feature of d electrons of Hf and finally give rise to magnetism in the system. In order to analyze the origin of the magnetism observed

above, we show in Fig. 4 the projected density of states (PDOS) of Hf_2C monolayer under different strains.

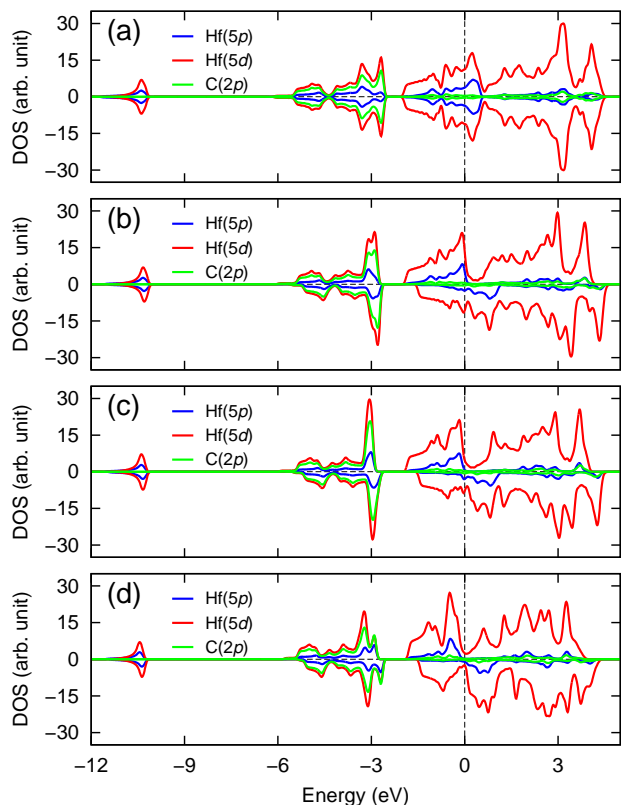


FIG. 4. Evolution of PDOS of Hf_2 along with biaxial symmetric strain: (a) 0.00%, (b) 1.56%, (c) 4.67% and (d) 7.78%.

It can be seen from Fig. 4(a) that the pristine Hf_2C is a metallic system where the energy states near the Fermi energy are mainly composed of $\text{Hf}(5d)$ orbitals. In the energy range from -5 to -2 eV, the states of $\text{C}(3p)$ and $\text{Hf}(5d)$ hybridize, forming bands separated by a gap of around 1eV from the $\text{Hf}(d)$ bands. The metallic nature of Hf_2C is not altered by applied strain since there are always bands crossing the Fermi level. However, the split of band is induced. The spin-up states of $\text{Hf}(5d)$ and $\text{Hf}(5p)$ start to shift towards lower energies, while the spin-down states shift towards higher energies. As a result, the magnetism is observed which is mainly contributed by the $\text{Hf}(5d)$ states. This magnetism is ascribed to the redistribution of atomic charges under external strain.

Closer examination of the PDOS reveals that the d_{yz} and d_{xz} states as well as d_{xy} and $d_{x^2-y^2}$ states of Hf are degenerated. The largest contribution for the magnetism is from the shift of d_{yz} and d_{xz} bands. This is in accordance with the biaxial strain we applied. Since the strain is symmetric, the degeneracy is not destroyed.

The spin density plot at a strain of 1.56% is provided in Fig. 5. At strain free state, there is no spin density in the Hf_2C monolayer, which is the reflection of its non-magnetic property. It is shown that the strain induced

ferromagnetism is mainly attributed the Hf since the unpaired spin electrons are mostly concentrated on the Hf atoms. Only a small fraction of spin density is located at C atoms. This is consistent with the results shown in the PDOS in Fig. 4.

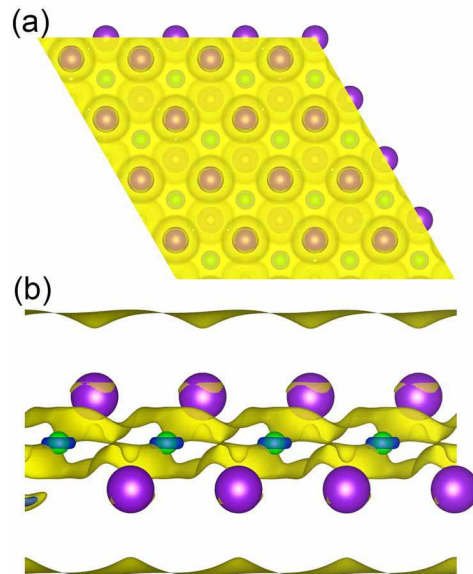


FIG. 5. The spin density distribution ($\rho_{\uparrow} - \rho_{\downarrow}$) with the positive portion denoted by yellow and negative denoted by blue. The isovalue is set to be $1 \times 10^{-4} \text{ e}/\text{\AA}^3$.

The spin-resolved band structure of Hf_2C under different biaxial strains is shown in Fig. 6, which clearly displays the opposite shift of Fermi level in the majority and minority spin bands when the strain is applied. As a consequence, the symmetric band structure becomes asymmetrical due to the shift of conduction and valence bands, in accordance with the DOS plot. The energy bands in the vicinity of Fermi level determines the magnetic behaviors as demonstrated above. The band splitting in this region changes Hf_2C to a magnetic metal.

The effects of spin-orbit coupling (SOC) on the calculated magnetism are also evaluated. With the unit cell of Hf_2C , we performed SOC calculations which treat magnetism noncollinearly using quantization axis (0, 0, 1) (i.e., z axis) based on the charge density from no SOC. Although the inclusion of SOC lowers the total energy about 1.42 eV, the calculated magnetic moment is not influenced. This result is in line with previous calculations regarding the effects of SOC on magnetic moment.²⁹ Therefore, our conclusion still holds irrespective of SOC.

We also checked the dependence of our results on the functional we have used so as to give more reliability of our results. In this case, we have performed a set of calculations about Hf_2C with PBE functional which has frequently used for the study of MXenes.^{24,25} The results indicate that the dependence of magnetic moments of Hf_2C on applied strain is more sensitive for PW91 than PBE

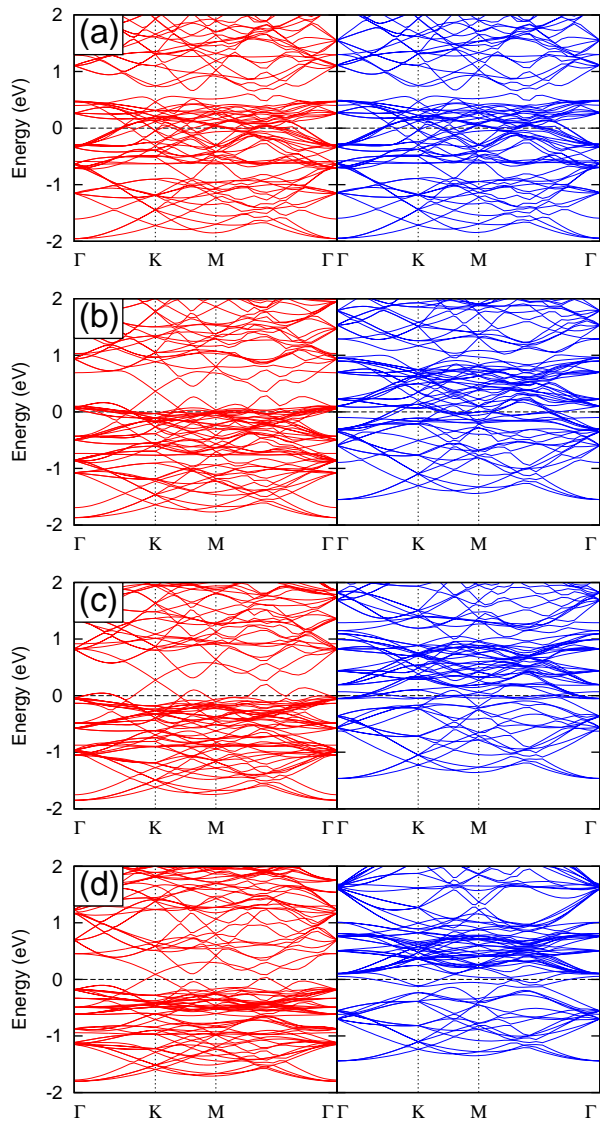


FIG. 6. Spin-resolved band structure of Hf_2 under different biaxial strains: (a) 0.00%, (b) 1.56%, (c) 4.67% and (d) 7.78%.

functional at small strains. Nevertheless, both function-

als predict a non-magnetic to magnetic transition when the strain is larger than 2%. Therefore, the main results discussed in this paper are not influenced.

Since the experimental synthesized MXenes are usually terminated with oxygen-containing and/or fluoride groups, we also examine the effect of strain on their electronic structures. The results show that all the MXenes considered exhibit no magnetism upon fictionalization. This conclusion is also found in Ti_2C in previous calculations.¹⁶ Our further simulation indicates that the nonmagnetic properties of H-, O- and F- functionalized Ti_2C monolayer is not changed along with applied strains.

In 2D materials, a conventional method to induce magnetism is to introduce vacancy or foreign atoms.^{30,31} However, the precise control of these structure is rather difficult experimentally. Besides, the generated magnetism in this way is often localized. Our results indicates that the magnetism of MXenes can be switched on and off facily by applied strains. In experiment, these strains can be achieved in a controlled manner, as demonstrated recently in 2D materials such as graphene.³² At strain-free state, only the Cr_2C are found to be magnetic among various MXenes, our results thus broaden the applicability of MXenes in future spintronics.

In summary, the electronic and magnetic properties of recently synthesized MXenes subjected to external biaxial symmetric strain are investigated by virtue of first-principles calculations based on density functional theory. All the considered MXenes are metallic in the strain-free state and the metallic characteristics are not influenced even with a large applied strains. Nevertheless, the magnetic moments of these MXenes are very sensitive to strains. Among the studied MXenes, the magnetic moment of Hf_2C exhibits a large variation which renders it magnetic with a magnetic moment of $1.5 \mu_B/\text{unit}$ at a strain of 1.80%. Our analysis reveals that the magnetism is originated from the shift of Hf(5d) bands. The present work provides a route to harness the magnetic properties of two-dimensional MXenes for spintronic applications.

ACKNOWLEDGMENTS

This work is financially supported by the NSFC (Grant No. 11274019).

* weikang@pku.edu.cn

¹ K. S. Novoselov, A. K. Geim, S. V. Morozov, D. Jiang, Y. Zhang, S. V. Dubonos, I. V. Grigorieva, and A. A. Firsov, *Science* **306**, 666 (2004).

² M. W. Barsoum, *Prog. Solid State Chem.* **28**, 201 (2000).

³ P. Eklund, M. Beckers, U. Jansson, H. Hberg, and L. Hultman, *Thin Solid Films* **518**, 1851 (2010).

⁴ M. W. Barsoum and M. Radovic, *Annu. Rev. Mater. Res.* **41**, 195 (2011).

⁵ X. Wang and Y. Zhou, *J. Mater. Sci. Technol.* **26**, 385 (2010).

⁶ M. Naguib, M. Kurtoglu, V. Presser, J. Lu, J. Niu, M. Heon, L. Hultman, Y. Gogotsi, and M. W. Barsoum, *Adv. Mater.* **23**, 4248 (2011).

⁷ M. Naguib, O. Mashtalir, J. Carle, V. Presser, J. Lu, L. Hultman, Y. Gogotsi, and M. W. Barsoum, *ACS Nano* **6**, 1322 (2012).

⁸ A. Enyashin and A. Ivanovskii, *Comput. Theor. Chem.*

- 989**, 27 (2012).
- ⁹ M. Naguib, J. Come, B. Dyatkin, V. Presser, P.-L. Taberna, P. Simon, M. W. Barsoum, and Y. Gogotsi, *Electrochem. Commun.* **16**, 61 (2012).
 - ¹⁰ Q. Tang, Z. Zhou, and P. Shen, *J. Amer. Chem. Soc.* **134**, 16909 (2012).
 - ¹¹ O. Mashtalir, M. Naguib, V. N. Mochalin, Y. DallAgnese, M. Heon, M. W. Barsoum, and Y. Gogotsi, *Nat. Comm.* **4**, 1716 (2013).
 - ¹² M. Khazaei, M. Arai, T. Sasaki, C.-Y. Chung, N. S. Venkataramanan, M. Estili, Y. Sakka, and Y. Kawazoe, *Adv. Funct. Mater.* **23**, 2185 (2013).
 - ¹³ N. J. Lane, M. W. Barsoum, and J. M. Rondinelli, *Europhys. Lett.* **101**, 57004 (2013).
 - ¹⁴ J. Come, M. Naguib, P. Rozier, M. W. Barsoum, Y. Gogotsi, P.-L. Taberna, M. Morcrette, and P. Simon, *J. Electrochem. Soc.* **159**, A1368 (2012).
 - ¹⁵ A. Enyashin and A. Ivanovskii, *J. Solid State Chem.* **207**, 42 (2013).
 - ¹⁶ Y. Xie and P. R. C. Kent, *Phys. Rev. B* **87**, 235441 (2013).
 - ¹⁷ W. S. Yun, S. W. Han, S. C. Hong, I. G. Kim, and J. D. Lee, *Phys. Rev. B* **85**, 033305 (2012).
 - ¹⁸ H. Peelaers and C. G. Van de Walle, *Phys. Rev. B* **86**, 241401 (2012).
 - ¹⁹ Y. Zhou, Z. Wang, P. Yang, X. Zu, L. Yang, X. Sun, and F. Gao, *ACS Nano* **6**, 9727 (2012).
 - ²⁰ V. M. Pereira, A. H. Castro Neto, and N. M. R. Peres, *Phys. Rev. B* **80**, 045401 (2009).
 - ²¹ G. Kresse and J. Furthmüller, *Phys. Rev. B* **54**, 11169 (1996).
 - ²² P. E. Blöchl, *Phys. Rev. B* **50**, 17953 (1994).
 - ²³ J. P. Perdew and Y. Wang, *Phys. Rev. B* **45**, 13244 (1992).
 - ²⁴ L.-Y. Gan, Y.-J. Zhao, D. Huang, and U. Schwingenschlögl, *Phys. Rev. B* **87**, 245307 (2013).
 - ²⁵ I. Shein and A. Ivanovskii, *Comput. Mater. Sci.* **65**, 104 (2012).
 - ²⁶ A. N. Enyashin and A. L. Ivanovskii, *J. Phys. Chem. C* **117**, 13637 (2013).
 - ²⁷ M. Kurtoglu, M. Naguib, Y. Gogotsi, and M. W. Barsoum, *MRS Comm.* **2**, 133 (2012).
 - ²⁸ J. A. Warner, S. K. R. Patil, S. V. Khare, and K. C. Masiulaniec, *Applied Physics Letters* **88**, 101911 (2006).
 - ²⁹ W. Xie, W. Xiong, C. A. Marianetti, and D. Morgan, *Phys. Rev. B* **88**, 235128 (2013).
 - ³⁰ P. O. Lehtinen, A. S. Foster, A. Ayuela, A. Krasheninnikov, K. Nordlund, and R. M. Nieminen, *Phys. Rev. Lett.* **91**, 017202 (2003).
 - ³¹ E. J. G. Santos, A. Ayuela, S. B. Fagan, J. Mendes Filho, D. L. Azevedo, A. G. Souza Filho, and D. Sánchez-Portal, *Phys. Rev. B* **78**, 195420 (2008).
 - ³² T. M. G. Mohiuddin, A. Lombardo, R. R. Nair, A. Bonetti, G. Savini, R. Jalil, N. Bonini, D. M. Basko, C. Galiotis, N. Marzari, K. S. Novoselov, A. K. Geim, and A. C. Ferrari, *Phys. Rev. B* **79**, 205433 (2009).
 - ³³ H. Shioya, M. F. Craciun, S. Russo, M. Yamamoto, and S. Tarucha, *Nano Lett.* (2014), DOI: 10.1021/nl403679f.